AIChE Letter: Separations: Materials, Devices and Processes

Multichannel Mixed-Conducting Hollow Fiber Membranes for Oxygen Separation

Jiawei Zhu, Ziye Dong, Zhengkun Liu, Kai Zhang, Guangru Zhang, and Wanqin Jin
State Key Laboratory of Materials-Oriented Chemical Engineering, College of Chemistry and Chemical engineering, Nanjing University of Technology, 5 Xinmofan Road, Nanjing 210009, P.R. China

DOI 10.1002/aic.14471
Published online April 19, 2014 in Wiley Online Library (wileyonlinelibrary.com)

Significance

A multichannel mixed-conducting hollow fiber (MMCHF) membrane, 0.5 wt % Nb_2O_5-doped $SrCo_{0.8}Fe_{0.2}O_{3-\delta}$ (SCFNb), has been successfully prepared by phase inversion and sintering technique. The crystalline structure, morphology, sintering behavior, breaking load, and oxygen permeability of the MMCHF membrane were studied systematically. The MMCHF membrane with porous-dense asymmetrical microstructure was obtained with the outer diameter of 2.46 mm and inner tetra-bore diameter of 0.80 mm. The breaking load of the MMCHF membrane was 3–6 times that of conventional single-channel mixed-conducting hollow fiber membrane. The MMCHF membrane showed a high oxygen flux which was about two times that of symmetric capillary membrane at similar conditions as well as a good long-term stability under low oxygen partial pressure atmosphere. This work proposed a new configuration for the mixed-conducting membranes, combining advantages of multichannel tubular membrane technology and conventional hollow fibers. © 2014 American Institute of Chemical Engineers *AIChE J*, 60: 1969–1976, 2014

Keywords: multichannel hollow fiber membrane, oxygen permeation, sintering behavior, mechanical strength, long-term stability

Introduction

Past decades have witnessed considerable research activities on mixed oxygen ionic and electronic conducting (MIEC) membranes due to their potential and wide applications in the separation of oxygen from air,[1,2] partial oxidation of light hydrocarbons,[3–5] fabrication of cathodes for solid oxide fuel cells,[6,7] as well as thermal decomposition of CO_2[8,9] and NO_x.[10] The MIEC membrane process and technique displays a large amount of significant advantages for oxygen separation from air over cryogenic air separation and pressure swing adsorption, containing simplicity of operation and other economic and environmental benefits.[11,12] However, several challenges, including chemistry and engineering issues, exist in developing MIEC membrane process and technique before large-scale industrial and commercial applications, such as promoting the oxygen permeability and mechanical strength. In order to solve these issues, many research efforts are directed toward not only advanced membrane materials with high performance but also optimization of the membrane configuration.

In most previous work, there are three main types of ceramic membrane configurations: plate, tube, and hollow fiber. Disk-shaped membranes are usually used for kinetic studies with limited membrane area because of simplified fabrication.[13,14] While a multiple planar stack can be used to enlarge the membrane area, many engineering difficulties such as sealing and connection appeared.[15] Tubular dense membranes prepared by paste extrusion with small surface/volume ratios and thick membrane walls causing low productivity of oxygen may restrict them in practical applications.[16,17] Alternatively, hollow fiber membranes fabricated by phase inversion and sintering technique possess a thin wall and an asymmetric structure and they can obtain high oxygen permeation flux. So the configuration of hollow fiber is considered as the most promising one for the future industrial application. Large research efforts concentrated on hollow fiber membranes because of their high oxygen permeation flux and high packing density.[18–25] Diniz da Costa coworkers[23] reported that the maximum oxygen flux of $Ba_{0.5}Sr_{0.5}Co_{0.8}Fe_{0.2}O_{3-\delta}$ hollow fiber membrane could reach 9.5 mL min^{-1} cm^{-2} at 1223 K. However, $Ba_{0.5}Sr_{0.5}Co_{0.8}Fe_{0.2}O_{3-\delta}$ is unstable over a period of 400 h at 1098 K because of the phase decomposition.[22] The $La_{0.6}Sr_{0.4}Co_{0.2}Fe_{0.8}O_{3-\delta}$ hollow fiber membrane showed a high oxygen permeation flux of 5.77 mL min^{-1} cm^{-2} at

Correspondence concerning this article should be addressed to W. Jin at wqjin@njut.edu.cn.

1323 K.[19] Unfortunately, the breaking load of the membrane is only about 1 N due to finger holes throughout the whole membrane wall.[19] Sunarso et al.[25] reported that the oxygen flux of $BaBi_{0.05}Sc_{0.1}Co_{0.15}O_{3-\delta}$.can reach 11.4 mL min^{-1} cm^{-2} at 1223 K. Nevertheless, the conventional single-channel mixed-conducting hollow fiber (SMCHF) membrane may not meet the requirements of industrialization, suffering from low mechanical strength. So far, no research relates to fabrication of multichannel inorganic hollow fiber membrane which may combine the advantages of multichannel tubular membrane technology[26,27] and conventional hollow fibers. The packing density, mechanical strength, permeation flux, energy efficiency, stability, and robustness in long-term operation may be improved by such configuration.

Therefore, the aim of this work is to develop a mixed-conducting membrane with multichannel hollow fiber configuration for oxygen separation. The multichannel mixed-conducting hollow fiber (MMCHF) membranes possessing good mechanical strength can be expected to overcome some drawbacks of SMCHF membranes. In our previous work, we found that $SrCo_{0.8}Fe_{0.2}O_{3-\delta}$ doped with 0.5 wt % of Nb_2O_5 (SCFNb) has high oxygen permeability, good chemical and structural stability, and low thermal expansion.[28] Herein, the SCFNb oxide was applied to construct the MMCHF membrane. The forming conditions, structure, breaking load, and oxygen permeability of the MMCHF membrane were studied in detail.

Experimental

Fabrication of SCFNb powder

The SCFNb oxides were synthesized by the conventional solid-state reaction method. Stoichiometric amount of $SrCO_3$ (99.9%), Co_2O_3 (99.9%), and Fe_2O_3 (99.9%) were mixed and ball-milled in ethanol for 24 h and then thermally treated at 523 K. The $SrCo_{0.8}Fe_{0.2}O_{3-\delta}$ (SCF) oxide was formed after a further calcination at 1173 K for 5 h in air. The SCFNb oxides were prepared by ball-mill mixing 0.5 wt % of Nb_2O_5 with the SCF powder for 24 h and then calcination at 1223 K for 5 h in air. For the spinning of MMCHF membranes, the SCFNb powder was grinded and sieved (300 meshes).

Preparation of MMCHF membranes

The MMCHF membranes were prepared via a combined phase inversion and sintering technique. The spinning suspension was composed of polyetherimide (PEI), 1-methyl-2-pyrrolidinone (NMP), and SCFNb powder in the mass ratio of 1:5:10. A specially designed tetra-bore spinneret with orifice diameter of 4.8 mm (the diameter of the four bores is 1.2 mm) was used to obtain the multichannel hollow fiber precursors. Deionized water were used as the internal and external coagulants, respectively. The formed precursor fibers were took out from water and then put in ethanol to avoid destruction of the SCFNb perovskite structure.[29] Afterward, the precursors were sintered at 1473 K for 10 h to remove the polymers and obtain the gas-tight membranes. The preparation conditions of obtaining the SCFNb MMCHF membrane are summarized in Table 1.

Table 1. Preparation Parameters for the SCFNb MMCHF Membranes

Parameter	Value
Composition of the spinning suspension	
SCFNb powder	62.5 wt %
PEI	6.25 wt %
NMP	31.25 wt %
Spinning temperature	293 K
Injection rate of internal coagulant	20 mL/min
Injection rate of suspension	20 mL/min
Air gap	15 cm
Sintering temperature	1473 K
Sintering time	10 h

Characterizations

The crystal phases of the as-prepared SCFNb powder and the fresh MMCHF membrane was characterized by X-ray diffraction (XRD, Bruker, model D8 Advance) using Cu Kα radiation. The diffraction patterns were collected at room temperature by step scanning at an increment of 0.05° in the range of $20° \leq 2\theta \leq 80°$. Morphology and microstructure of the MMCHF membranes were visually observed via a scanning electron microscope (SEM, Hitachi S-4800, Japan). The composition of the membrane materials was verified by energy dispersive X-ray spectroscopy (EDX, Hitachi S-4800, Japan).

The sintering behavior of the MMCHF precursor was measured in the air atmosphere using the apparatus of dilatometer (Netzsch, Model DIL 402C). The specimen was 2 mm length. The shrinkage measurement was performed in the range from room temperature to 1513 K with heating rates of 5 K min^{-1}. The dilatometer was calibrated using sapphire as a standard specimen.

The mechanical strength of the MMCHF membrane was measured through a three-point bending test performed using a tensile (Model CMT6203) provided with a load cell for 5 kN. The hollow-fiber samples were fixed in the sample holder with a spec gauge length of 50 mm. The crosshead speed was set at 0.02 cm min^{-1}. The load (F_m) needed to break the hollow fiber was recorded for each sample.

Oxygen permeation measurement

Oxygen permeation fluxes of the dense MMCHF membranes without any defects were measured in a high temperature membrane cell, as can be seen in our previous work.[30,31] A MMCHF membrane with the length of 30 mm was sealed with the two dense Al_2O_3 ceramic tubes. The sealing part is inside the furnace and the sealing method in our experiment is high-temperature sealing. A quartz tube around the two alumina tubes formed the shell side of the membrane. Air was fed to the shell side while He swept on the lumen side to carry the permeated oxygen through the membrane. The inlet gas flow rates were controlled by mass flow controllers (model D07-19B). Both sides of the membrane were maintained at the pressure of 1 bar. A programmable temperature controller (Model AI-708PA, Xiamen Yudian automation technology Co.) monitored the temperature surrounding the membrane. The operating temperature in this work was considered as the center temperature of the

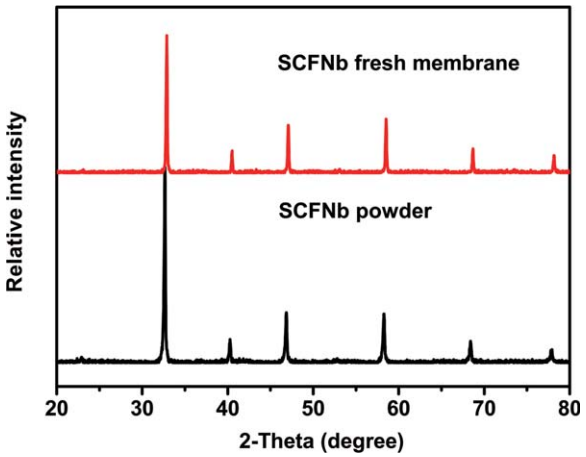

Figure 1. XRD patterns of SCFNb powder and fresh membrane.

[Color figure can be viewed in the online issue, which is available at wileyonlinelibrary.com.]

furnace. The composition of effluent streams from the lumen side was analyzed by an on-line gas chromatograph (GC, Shimadzu, model GC-8A, Japan). The leakage of oxygen due to the impact sealing was usually less than 0.5% of the total oxygen permeation flux during the experiments. Assuming that leakage of nitrogen and oxygen through pores or cracks in accordance with Knudsen diffusion,[30,32] the fluxes of leaked N_2 and O_2 are related by $J_{N_2}:J_{O_2}=(32/28)^{0.5}\times 79/21=4.02$. Then, the oxygen permeation flux was calculated as follows

$$J_{O_2}(\mathrm{mL}\times\mathrm{min}^{-1}\times\mathrm{cm}^{-2})=(C_{O_2}-C_{N_2}/4.02)\times Q/S \quad (1)$$

Where C_{O_2} and C_{N_2} are the concentration of oxygen and nitrogen calculated from the GC measurements, Q (mL min^{-1}) is the flow rate of the permeate gas stream, and S (cm^2) is simply defined as the membrane outer surface area due to the complex structure of the MMCHF membranes.

Results and Discussion

Crystalline structure and composition of the MMCHF membrane

Figure 1 compared the XRD patterns of the sintered MMCHF membrane and the original powder. It can be seen that both the SCFNb powder and SCFNb MMCHF membrane (ground into powder for the analysis) maintained a perovskite crystalline structure and no secondary phase.[28] The peaks of sintered MMCHF membrane slightly shift toward higher 2-theta values in comparison with the original SCFNb powder. Such a change indicates that the lattice diameter decreases with slight change in material compositions during the wet spinning and sintering process, which is in agreement with EDX analysis listed in Table 2. Similar results were found in our previous work.[29]

Morphology of the MMCHF membrane

Figure 2 is the image of the MMCHF precursor and the sintered MMCHF membrane. Both the MMCHF precursor and the sintered MMCHF membrane have well-formed tetrabore structure. The morphologies of the MMCHF precursor and the MMCHF membrane are shown in Figure 3. Figures 3a,c show that the outer and inner diameters of the MMCHF precursor and the sintered MMCHF membrane were shrunk from about 3.52 and 1.11 mm to 2.46 and 0.80 mm, respectively. The MMCHF membrane can provide a large membrane area per unit packing volume of 1630 $\mathrm{m}^2\ \mathrm{m}^{-3}$. Because the structure of the MMCHF membranes is complex, the real membrane area is hard to define. Herein, the membrane area is simply defined as the outer surface area of the MMCHF membrane. The wall structure of the MMCHF precursor is displayed in Figure 3b. Finger like pores are exhibited near the inner wall of the MMCHF precursor and that sponge like structures appear at the center wall of the MMCHF precursor. After sintering, the wall structure of the MMCHF precursor is well maintained as shown in Figures 3d,e. Figure 3f clearly shows that the thickness of the membrane dense layer is about 10 μm. The formation of the multichannel hollow fiber wall structures is tied to the complicated interactions among solvent, nonsolvent and binder during the phase inversion process. In detail, the formation of dense layers may be resulted from rapid exchanging between the solvent and nonsolvent at the inner and outer walls, while the formation of sponge-like or finger like pores may be attributed to slow solvent and nonsolvent diffusion out of the center of the walls. Figure 3g,h depict the outer surface and inner surface of the sintered MMCHF membrane, respectively. The dense structure on the

Table 2. EDX Results of SCFNb Powder and Sintered Membrane

	Powder (mole %)	Sintered membrane (mole %)	Theoretical value (mole %)
Sr	48.32	45.86	49.82
Co	41.15	43.52	39.85
Fe	10.12	9.93	9.96
Nb	0.41	0.69	0.37

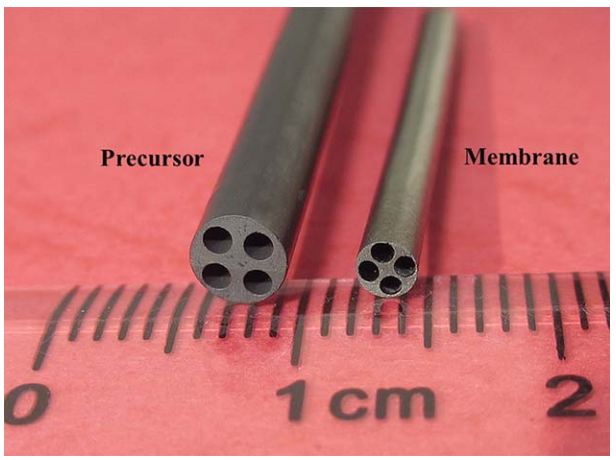

Figure 2. Image of the MMCHF precursor and sintered MMCHF membrane.

[Color figure can be viewed in the online issue, which is available at wileyonlinelibrary.com.]

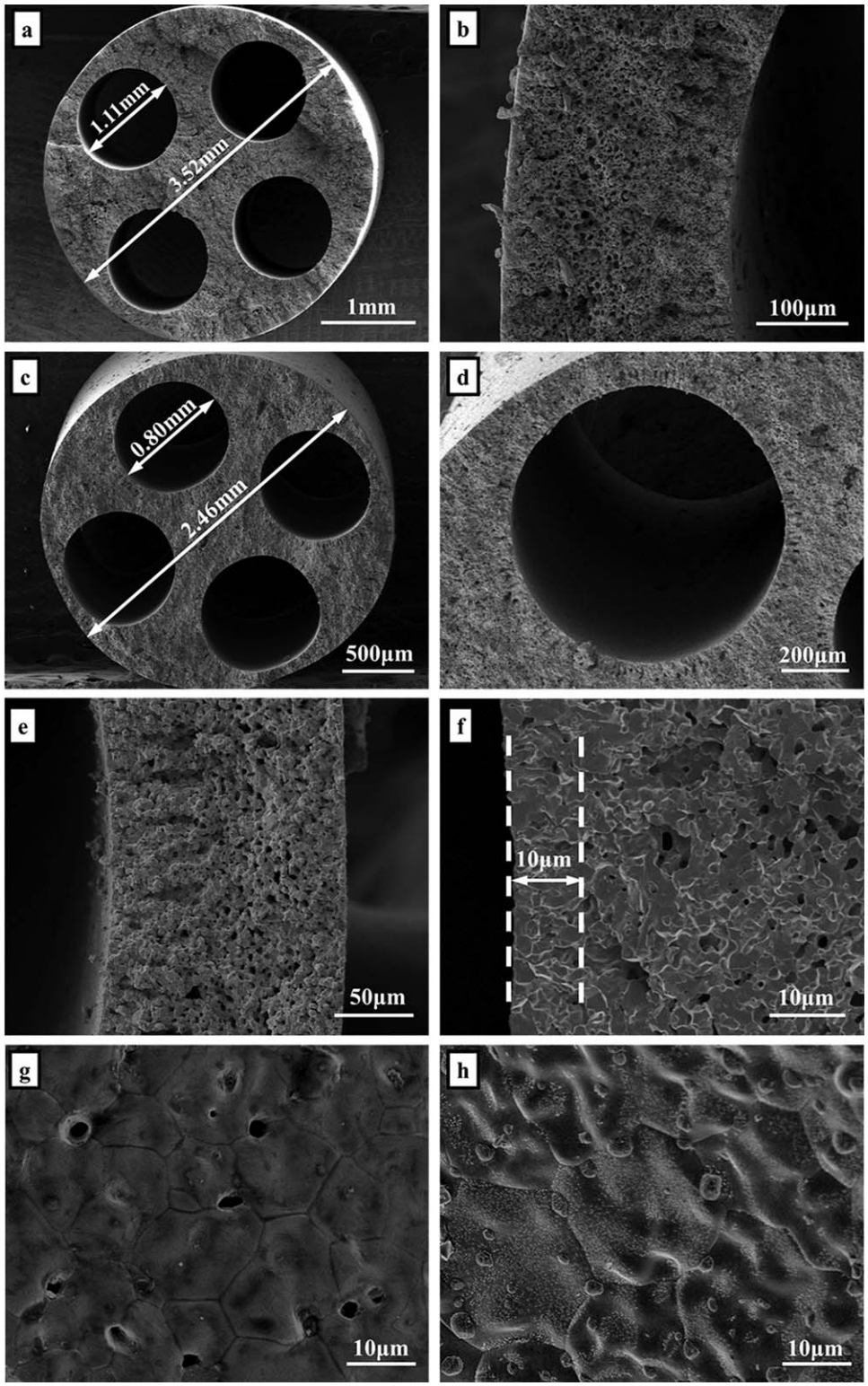

Figure 3. SEM images of the MMCHF precursor and sintered MMCHF membrane.

(a) Cross section of the precursor; (b) wall of the precursor; (c) cross section of the sintered membrane; (d) lower magnification of the sintered membrane cross section; (e) the wall of the sintered membrane; (f) magnification of the sintered membrane wall; (g) outer surface of the sintered membrane; and (h) inner surface of the sintered membrane.

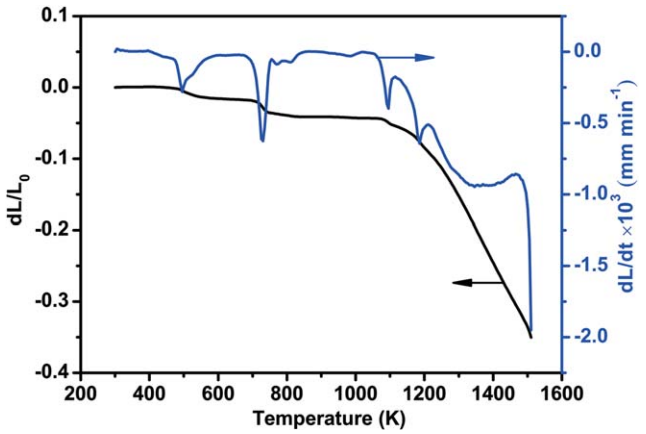

Figure 4. Temperature dependence of shrinkage and shrinkage rate of the MMCHF membrane.

[Color figure can be viewed in the online issue, which is available at wileyonlinelibrary.com.]

membrane inner surface was formed upon sintering. Due to the pores in the cross section of the membrane shown in Figure 3e are not connected, the membrane is dense and gas-tight. Although there are some pores still present on the outer surfaces, they did not affect the gas-tightness property of the membrane.

Sintering behavior of the MMCHF membrane

For ceramic hollow fiber membranes normally with complex structures, the sintering process is also very complex.[33] So it is very necessary to study the sintering behavior of the MMCHF membrane. The sintering behavior of the MMCHF membrane in the air atmosphere is shown in Figure 4. The linear shrinkage of the multichannel hollow fiber is about 31.2% at the sintering temperature of 1473 K. Additionally, an inflection point is observed at 1483 K. This indicates that the sintering process of the MMCHF membrane is completed at about 1483 K. In the temperature range of 301–1123 K, the hollow fiber membrane hardly shows the sintering ability. The shrinkage of the membrane is due to the burning process of the polymer binder. In the temperature range of 1123–1373 K, the membrane begun to sinter and the shrinkage rate increased sharply with increasing temperature, where shrinkage rate was defined as dL/dt (L is the length of membrane sample; t is the heat time of dilatometer). The shrinkage rate curve shows that the maximum value of the shrinkage rate is at 1373 K. The phenomenon of sample shrinkage is caused by the growth of neck between the particles. In the temperature range of 1373–1483 K, the shrinkage rate decreases with increasing the temperature. When the temperature is higher than 1483 K, the rate curve drops quickly. This may be caused by the melting of the membrane material. So the sintering temperature range of the MMCHF membrane is about 1373–1483 K. And we found that the membrane sintered at 1473 K for 10 h is gas-tight and dense according to our gas-tight test. The gas-tightness of membranes was checked by purified nitrogen at room temperature. The nitrogen with an absolute pressure up to 0.2 MPa was fed into the lumen side of the membrane and the permeation of nitrogen was not detected at shell side of the membrane.

Mechanical property of the MMCHF membrane

The mechanical property (breaking load) of ceramic hollow fiber membranes is an important parameter for their industrial application. In fabrication of ceramic hollow fiber membranes, the cross section structure may play one of the most important roles for achieving a better value of breaking load. In this work, the breaking load of the MMCHF membrane was investigated. As shown in Table 3, the MMCHF membrane can withstand a breaking load of 3.83 ± 0.23 N, which is much better than those of single-channel fibers (The breaking load of the references can be calculated by the following equation

$$F_m = \pi\sigma_F(D^4 - d^4)/8LD \quad (2)$$

where σF is the bending strength reported by the references[19,23,24,34]; D and d are the outer diameter (OD) and the inner side diameter (ID) of the reported SMCHF, respectively; L is the length of the SMCHF fixed at 5 cm. Although the breaking load of the membrane may be related to the fabrication conditions and the properties of the membrane material, the good breaking load value of the MMCHF membrane mainly attributed to the special crucifix shape

Table 3. Comparison of the Breaking Load between SMCHFs and MMCHF Membrane

Geometries	Membrane materials	Character (mm)	F_m (N)	References
SMCHF	$BaCo_xFe_yZr_zO_{3-\delta}$	OD = 0.88 ID = 0.53	0.81	24
SMCHF	$La_{0.6}Sr_{0.4}Co_{0.2}Fe_{0.8}O_{3-\delta}$	OD = 1.28 ID = 1.11	0.79	19
SMCHF	$La_{0.6}Sr_{0.4}Co_{0.2}Fe_{0.8}O_{3-\delta}$	OD = 1.40 ID = 1.18	1.21	19
SMCHF	$SrCe_{0.95}Y_{0.05}O_{2.975}$	OD= 1.31 ID = 0.83	0.76	34
SMCHF	$SrCe_{0.95}Y_{0.05}O_{2.975}$	OD = 1.26 ID = 0.94	0.65	34
SMCHF	$SrCe_{0.95}Y_{0.05}O_{2.975}$	OD = 1.25 ID = 0.97	0.5	34
SMCHF	$Ba_{0.5}S_{r0.5}Co_{0.8}Fe_{0.2}O_{3-\delta}$	OD = 1 ID = 0.36	0.75 ± 0.12	23
MMCHF	SCFNb	OD = 2.46 ID = 0.80	3.83 ± 0.23	This work

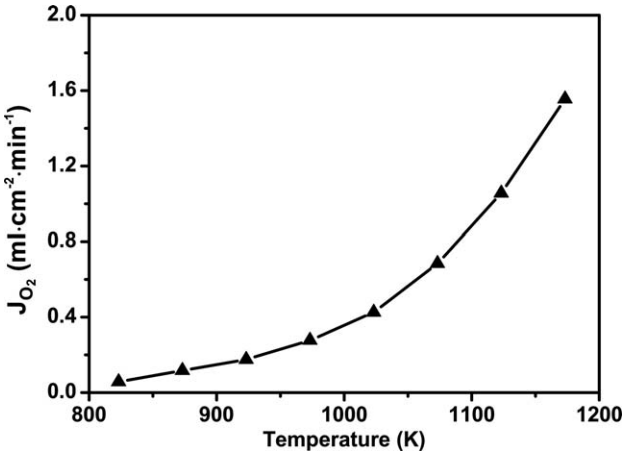

Figure 5. Oxygen permeation flux through the MMCHF membrane as a function of temperature ($F_{Air} = 180$ mL min^{-1}, $F_{He} = 80$ mL min^{-1}).

structure, which can play a supporting role in bearing the force applied on the membrane. So the MMCHF membranes have great potential for practical application.

Oxygen permeability of the MMCHF membrane

Oxygen permeation tests of the MMCHF membrane were performed to investigate the effect of operating conditions such as temperature, air flow rate, and sweep gas flow rate.

The temperature dependence of oxygen permeation flux through the membrane was studied between 823 and 1173 K. The flow rates of air and helium were 180 mL min^{-1} and 80 mL min^{-1}, respectively. As shown in Figure 5, the oxygen permeation flux increases significantly with rising temperature due to the improvement of the oxygen bulk diffusion and the oxygen surface reaction rates. When the temperature increases from 823 to 1173 K, the oxygen permeation flux rises from 0.06 to 1.56 mL min^{-1} cm^{-2}, although the oxygen partial pressure on the permeate side also increases simultaneously. In other words, the operating temperature plays a more significant role in the oxygen permeation than the concentration driving force for the MMCHF membrane.

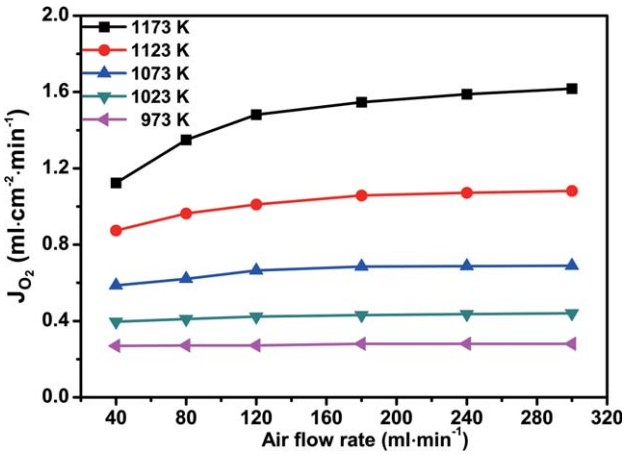

Figure 6. Effect of air flow rates on the oxygen permeation flux through the MMCHF membrane at different temperatures ($F_{He} = 80$ mL min^{-1}).

[Color figure can be viewed in the online issue, which is available at wileyonlinelibrary.com.]

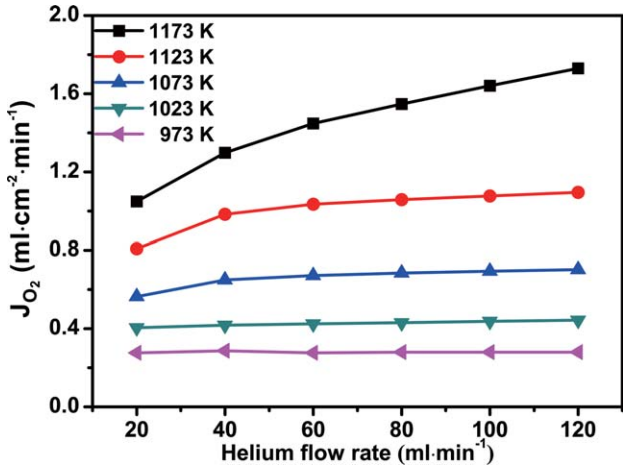

Figure 7. Effect of helium flow rates on the oxygen permeation flux through the MMCHF membrane at different temperatures ($F_{Air} = 180$ mL min^{-1}).

[Color figure can be viewed in the online issue, which is available at wileyonlinelibrary.com.]

Figure 6 shows oxygen permeation flux as a function of air flow rate at different operating temperatures. The flow rate of helium at the permeate side was fixed at 80 mL min^{-1}. At 1173 K, the oxygen permeation fluxes increase with increasing air flow rate. It was found that the oxygen flow rate increased sharply up to an air flow rate of 120 mL min^{-1}, while a further increase of air flow rate only slightly increases the oxygen permeation flux. When the operating temperature is below 1073 K, the oxygen flow rate increases with the increase of air flow rate at first, then keeps constant as the air flow rate is higher than 120 mL min^{-1}. These results indicate that the oxygen permeation flux is more sensitive to air flow rate at a higher operating temperature. To obtain high oxygen permeation flux of the MMCHF membrane, the feed air should be offered to operation unit abundantly.

The influence of the helium sweep flow rates at the permeate side on the oxygen permeation flux through the MMCHF membrane at different temperature is shown in Figure 7, while the air flow rate is kept constant of 180 mL min^{-1}. The helium flow rate varied from 20 to 120 mL min^{-1} in this experiment. As expected, the oxygen permeation fluxes through the MMCHF membrane increased with increasing the helium flow rate because the high helium flow rate lowered the oxygen partial pressure at the lumen side. For instance, at 1173 K, when the helium flow rate increases from 20 to 120 mL min^{-1}, the oxygen permeation flux increases from 1.06 to 1.72 mL min^{-1} cm^{-2}. For a symmetric capillary SCFNb membrane, Wu et al.[29] reported oxygen permeation fluxes of 0.19 mL min^{-1} cm^{-2} at 1073 K. Under the similar conditions, the rate measured in this work was 0.36 mL min^{-1} cm^{-2}. The possible reasons could be the following: the wall of the MMCHF membrane is thinner than that of the symmetric capillary membrane. Moreover, MMCHF membrane fabricated in this study had a porous-dense asymmetrical microstructure, whereas the symmetric

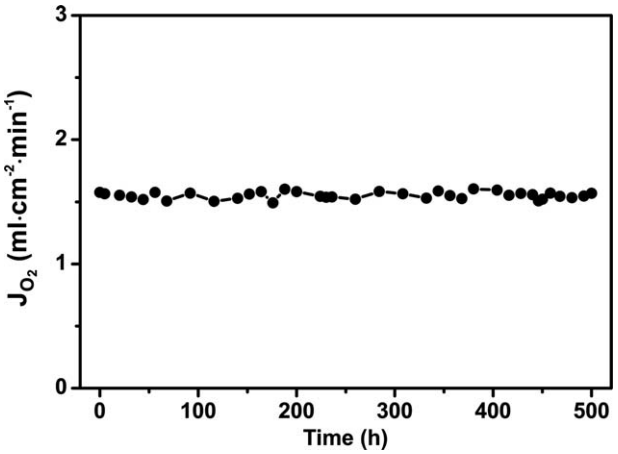

Figure 8. Long-term stability of the MMCHF membrane (temperature = 1173 K, F_{Air} = 180 mL min^{-1}, F_{He} = 80 mL min^{-1}).

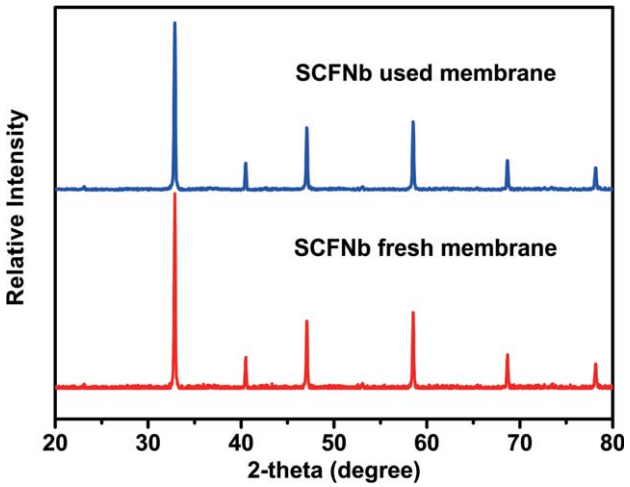

Figure 9. XRD patterns of the used MMCHF membrane.

[Color figure can be viewed in the online issue, which is available at wileyonlinelibrary.com.]

capillary membrane reported by Wu et al.[29] was totally dense.

For industrial applications, the membrane for oxygen separation should not only have high oxygen permeability, but also possess a good stability for a long time operation. Figure 8 shows the oxygen permeation stability of MMCHF membrane at 1173 K with air flow rate of 180 mL min^{-1} and helium flow rate of 80 mL min^{-1} on the lumen side. A generally steady oxygen permeation flux of 1.56 mL min^{-1} cm^{-2} was obtained at 1173 K during 500 h operation. Figure 9 compares the XRD patterns of the used membrane and the fresh membrane. We can find that the pervoskite structure of SCFNb is well maintained after the 500 h test. These results indicate that the MMCHF membrane contains good stability during the oxygen permeation test.

Conclusions

The MMCHF membrane with an asymmetrical microstructure was successfully prepared by phase inversion and sintering technique, combining advantages of multichannel tubular membrane technology and conventional hollow fibers. The MMCHF membrane sintered at 1473 K for 10 h was gas-tight and dense with outer diameter of 2.46 mm and inner tetra-bore diameter of 0.80 mm. The prepared MMCHF membrane exhibited a breaking load value of 3.83 ± 0.23 N which was about 3–6 times that of SMCHFs and an oxygen permeation flux which was about twice that of the symmetric capillary membrane at 1073 K. Long-term oxygen permeation test (1173 K, 500 h) showed that the MMCHF membranes possess good stability under low oxygen partial pressure atmosphere. Our work not only demonstrates that the MMCHF membrane can be a competitive candidate for industrial application, but also provides a strategy to simultaneously improve membrane structure stability and membrane permeation flux.

Acknowledgment

This work was supported by the Innovative Research Team Program by the Ministry of Education of China (No. IRT13070).

Literature Cited

1. Tan XY, Liu YT, Li K. Mixed conducting ceramic hollow-fiber membranes for air separation. *AIChE J*. 2005;51:1991–2000.
2. Tablet C, Grubert G, Wang HH, Schiestel T, Schroeder M, Langanke B, Caro J. Oxygen permeation study of perovskite hollow fiber membranes. *Catal Today*. 2005; 104:126–130.
3. Jin W, Gu X, Li S, Huang P, Xu N, Shi J. Experimental and simulation study on a catalyst packed tubular dense membrane reactor for partial oxidation of methane to syngas. *Chem Eng Sci*. 2000;55:2617–2625.
4. Tan XY, Li K. Oxidative coupling of methane in a perovskite hollow-fiber membrane reactor. *Ind Eng Chem Res*. 2006;45:142–149.
5. Jiang HQ, Wang HH, Werth S, Schiestel T, Caro J. Simultaneous production of hydrogen and synthesis gas by combining water splitting with partial oxidation of methane in a hollow-fiber membrane reactor. *Angew Chem Int Ed*. 2008;47:9341–9344.
6. Shao ZP, Haile SM. A high-performance cathode for the next generation of solid-oxide fuel cells. *Nature*. 2004; 431:170–173.
7. Zhou W, Ran R, Shao ZP. Progress in understanding and development of $Ba_{0.5}Sr_{0.5}Co_{0.8}Fe_{0.2}O_{3-\delta}$-based cathodes for intermediate-temperature solid-oxide fuel cells: A review. *J Power Sources*. 2009;192:231–246.
8. Jin WQ, Zhang C, Zhang P, Fan YQ, Xu NP. Thermal decomposition of carbon dioxide coupled with POM in a membrane reactor. *AIChE J*. 2006;52:2545–2550.
9. Jin WQ, Zhang C, Chang XF, Fan YQ, Xing WH, Xu NP. Efficient catalytic decomposition of CO_2 to CO and O_2 over Pd/mixed-conducting oxide catalyst in an oxygen-permeable membrane reactor. *Environ Sci Technol*. 2008;42:3064–3068.
10. Jiang HQ, Wang HH, Liang FY, Werth S, Schiestel T, Caro J. Direct decomposition of nitrous oxide to nitrogen by in situ oxygen removal with a perovskite membrane. *Angew Chem Int Ed*. 2009;48:2983–2986.

11. Hashim SS, Mohamed AR, Bhatia S. Oxygen separation from air using ceramic-based membrane technology for sustainable fuel production and power generation. *Renew Sust Energ Rev*. 2011;15:1284–1293.
12. Stiegel GJ, Maxwell RC. Gasification technologies: the path to clean, affordable energy in the 21st century. *Fuel Process Technol*. 2001;71:79–97.
13. Li SG, Jin WQ, Huang P, Xu NP, Shi J, Hu MZC, Payzant EA, Ma YH. Perovskite-related ZrO_2-doped $SrCo_{0.4}Fe_{0.6}O_{3-\delta}$ membrane for oxygen permeation. *AIChE J*. 1999;45(2):276–284.
14. Zeng Y, Lin YS, Swartz SL. Perovskite-type ceramic membrane: synthesis, oxygen permeation and membrane reactor performance for oxidative coupling of methane. *J Member Sci*. 1998;150:87–98.
15. Dyer PN, Richards RE, Russek SL, Taylor DM. Ion transport membrane technology for oxygen separation and syngas production. *Solid State Ionics*. 2000;134:21–33.
16. Wang HH, Wang R, Liang DT, Yang WS. Experimental and modeling studies on $Ba_{0.5}Sr_{0.5}Co_{0.8}Fe_{0.2}O_{3-\delta}$ (BSCF) tubular membranes for air separation. *J Member Sci*. 2004;243:405–415.
17. Jin WQ, Li SG, Huang P, Xu NP, Shi J, Lin YS. Tubular lanthanum cobaltite perovskite-type membrane reactors for partial oxidation of methane to syngas. *J Member Sci*. 2000;166:13–22.
18. Tan XY, Liu YT, Li K. Preparation of LSCF ceramic hollow-fiber membranes for oxygen production by a phase-inversion/sintering technique. *Ind Eng Chem Res*. 2005;44:61–66.
19. Zydorczak B, Wu ZT, Li K. Fabrication of ultrathin $La_{0.6}Sr_{0.4}Co_{0.2}Fe_{0.8}O_{3-\delta}$ hollow fibre membranes for oxygen permeation. *Chem Eng Sci*. 2009;64:4383–4388.
20. Tan XY, Wang ZG, Meng B, Meng XX, Li K. Pilot-scale production of oxygen from air using perovskite hollow fibre membranes. *J Member Sci*. 2010;352:189–196.
21. Liu SM, Gavalas GR. Oxygen selective ceramic hollow fiber membranes. *J Member Sci*. 2005;246:103–108.
22. Shao ZP, Yang WS, Cong Y, Dong H, Tong JH, Xiong GX. Investigation of the permeation behavior and stability of a $Ba_{0.5}Sr_{0.5}Co_{0.8}Fe_{0.2}O_{3-\delta}$oxygen membrane. *J Member Sci*. 2000;172:177–188.
23. Leo A, Smart S, Liu S, da Costa JCD. High performance perovskite hollow fibres for oxygen separation. *J Member Sci*. 2011;368:64–68.
24. Schiestel T, Kilgus M, Peter S, Caspary KJ, Wang H, Caro J. Hollow fibre perovskite membranes for oxygen separation. *J Member Sci*. 2005;258:1–4.
25. Sunarso J, Liu S, Lin YS, da Costa JCD. High performance BaBiScCo hollow fibre membranes for oxygen transport. *Energ Environ Sci*. 2011;4:2516–2519.
26. Mulder M. Basic Principles of Membrane Technology, 2nd ed. Dordrecht: Kluwer Academic Publishers, 1996.
27. Ghosh S, Bhattacharya P, Majumdar S, Dasgupta S, Bandyopadhyay S. Comparative study on treatment of kitchen-sink wastewater using single and multichannel ceramic membrane. *Int J Environ Tech Manag*. 2010;13:336–347.
28. Zhang GR, Liu ZK, Zhu N, Jiang W, Dong XL, Jin WQ. A novel Nb_2O_5-doped $SrCo_{0.8}Fe_{0.2}O_{3-\delta}$ oxide with high permeability and stability for oxygen separation. *J Member Sci*. 2012;405:300–309.
29. Wu ZT, Othman NH, Zhang GR, Liu ZK, Jin WQ, Li K. Effects of fabrication processes on oxygen permeation of Nb_2O_5-doped $SrCo_{0.8}Fe_{0.2}O_{3-\delta}$ micro-tubular membranes. *J Member Sci*. 2013;442:1–7.
30. Liu ZK, Zhang GR, Dong XL, Jiang W, Jin WQ, Xu NP. Fabrication of asymmetric tubular mixed-conducting dense membranes by a combined spin-spraying and co-sintering process. *J Member Sci*. 2012;415:313–319.
31. Zhang C, Xu Z, Chang XF, Zhang ZC, Jin WQ. Preparation and characterization of mixed-conducting thin tubular membrane. *J Member Sci*. 2007;299:261–267.
32. Wei YY, Liu HF, Xue JA, Li Z, Wang HH. Preparation and oxygen permeation of U-shaped perovskite hollow-fiber membranes. *AIChE J*. 2011;57:975–984.
33. Tan XY, Wang ZG, Li K. Effects of sintering on the properties of $La_{0.6}Sr_{0.4}Co_{0.2}Fe_{0.8}O_{3-\delta}$ perovskite hollow fiber membranes. *Ind Eng Chem Res*. 2010;49:2895–2901.
34. Liu SM, Tan XY, Li K, Hughes R. Preparation and characterisation of $SrCe_{0.95}Yb_{0.05}O_{2.975}$ hollow fibre membranes. *J Member Sci*. 2001;193:249–260.

Received Jan. 13, 2014, and revision received Mar. 7, 2014.